Sound-Wave–Soft-Mode Interaction near Displacive Phase Transitions: Spin Reorientation in $ErFeO_3$ †

G. Gorodetsky* and B. Lüthi
Department of Physics, Rutgers University, New Brunswick, New Jersey 08903
(Received 4 May 1970)

We present experimental and theoretical results of the sound-wave–spin-wave interaction in the spin reorientation region for the orthoferrite $ErFeO_3$. Near the transition temperatures $T_l = 87$ °K and $T_u = 96.6$ °K, a longitudinal sound wave propagating along the c axis exhibits a sound-wave–order-parameter interaction which is linear in the strain and quadratic in the order parameter. This leads to steplike discontinuities in the sound velocity. The experimentally observed velocity change at T_l and T_u is 0.8%. This gives a magnetoelastic coupling constant of $|B_{33}-B_{31}| \sim 18\times10^6$ erg/cm^3. Attenuation peaks at T_l and T_u arise from the same resonant interaction. Shear waves, with polarization vector along the a axis, exhibit velocity dips at T_l and T_u indicating an interaction linear in the strain and the order parameter. A theoretical fit to the velocity curve yields the magnetoelastic coupling constant $|B_{55}| = 2.2\times10^6$ erg/cm^3. Again, spin-wave damping leads to attenuation peaks at T_l and T_u. Finally, shear waves, with polarization vector along the b axis, do not give any coupling to the order parameter, but only a coupling to the optical branch of the spin-wave spectrum. This leads to a small noticeable sound-wave velocity change in the spin reorientation region. All these effects can be quantitatively described by a linearized set of coupled spin-wave and sound-wave equations of motion.

I. INTRODUCTION

Sound propagation near phase transitions has received considerable attention recently.[1] Near order-disorder phase transition (e.g., a ferro- or antiferromagnetic-paramagnetic transition) the sound wave couples to the fluctuations (spin fluctuation or spin energy density fluctuations in the case of magnetic transitions), producing large critical attenuation peaks and noticeable velocity changes, which are only partly quantitatively understood so far.[2]

For displacive phase transitions, the situation is quite different. In this case the fluctuations are rather small, except in a small temperature region close to T_a, the phase-transition temperature.[3] Near such a phase transition one observes mainly resonant interactions between the phonon and the soft mode (one-phonon–one-soft-mode processes) giving rise to pronounced sound-velocity changes and attenuation peaks, but not to critical effects due to fluctuations. These characteristic effects for displacive-type phase transitions are negligible near order-disorder phase transitions because the rather large fluctuations in the latter case overshadow all resonant sound-wave–soft-mode interactions.

In this paper we should like to show experimental results for a variety of effects due to the phonon–soft-mode resonant interaction for a typical displacive-type phase transition, the spin reorientation phase transition occurring in the orthoferrite $ErFeO_3$.[4] The magnetoelastic interaction allows different types of coupling for the different sound-wave modes; namely, a sound-wave-order-parameter coupling which is quadratic or linear in the order parameter. In each case we observe characteristic velocity and attenuation effects which can be quantitatively accounted for.

The spin reorientation phase transitions in the orthoferrites are typical examples for displacive Landau-type transitions where fluctuation effects are negligible.[5] Under the action of different temperature-dependent anisotropy energies the weak ferromagnetic moment rotates[6] from the orthorhombic c axis at T_u to the orthorhombic a axis at T_l ($T_u > T_l$). This rotation occurs in the ac plane due to a large asymmetric Dzyaloshinsky-type exchange interaction whose vector $\vec{D}$ is perpendicular to the ac plane.[4] An energy density expression of the form

$$E_\theta = \tfrac{1}{2}K_u \cos 2\theta + K_b \cos 4\theta \qquad (1)$$

is sufficient to describe the statics of such a phase transition. θ is the angle between the c axis and the weak ferromagnetic moment $\vec{m}$, K_u and K_b are the twofold and fourfold anisotropy constants discussed below. For $K_b > 0$, $\vec{m}$ changes continuously from the c to the a axis upon lowering the temperature, whereas for $K_b < 0$, $\vec{m}$ jumps discontinuously from the c to the a axis, giving rise to hysteresis, characteristic for first-order phase transitions. For the bulk of the sample it is found that the spin reorientation proceeds continuously in this temperature region for $ErFeO_3$,[6] indicating $K_b > 0$. Furthermore, it is found experimentally[7] that K_b is rather weakly

dependent on temperature, whereas K_u varies roughly linearly with T for $T \sim T_u$, T_l, for $SmFeO_3$. One can readily obtain the static properties of this phase transition by calculating $\partial E/\partial\theta$ and $\partial^2 E/\partial\theta^2$ from Eq. (1). For $K_b > 0$ one finds

$$\begin{aligned} T \geq T_u: &\quad \sin\theta = 0, && -K_u \geq 8K_b \\ T_l < T < T_u: &\quad \cos 2\theta = -K_u/8K_b, && 64K_b^2 > K_u^2 \\ T \leq T_l: &\quad \cos\theta = 0, && K_u \geq 8K_b \,. \end{aligned} \tag{2}$$

The equal signs in the stability expressions define T_u and T_l. From Eq. (2) it follows that the appropriate order parameter is the angle θ for T near T_u and $\frac{1}{2}\pi - \theta$ for T near T_l.

Associated with these phase transitions is the occurrence of a soft mode, in this case the $k = 0$ spin-wave mode of the acoustic branch. This mode has been calculated by various authors.[8–10] It shows (for zero external field) the characteristic features of a soft mode. It goes to zero at T_l and T_u, thus giving rise to an instability in the spin system.

It is mainly the interaction of a sound wave with this soft spin-wave mode which we consider in this paper. The sound-wave–spin-wave coupling is naturally of the linear magnetoelastic type, since the spin reorientation is driven by anisotropy energies. This is in contrast to the paramagnetic-ferromagnetic phase transition, where the dominant coupling mechanism is usually of the volume magnetostrictive type.[2]

In Sec. II we first deal with the particular form of the magnetoelastic coupling permitted by symmetry. Then we present a simple theoretical description for the expected velocity changes. Finally we give a rather rigorous presentation of the equation of motion method, solving for the coupled spin-wave–phonon modes. In the following sections we describe the experimental setup and then present the results for the sound-velocity and sound-attenuation changes. We will give a quantitative comparison of experimental and theoretical results.

II. THEORY

A. Magnetoelastic Interaction

The magnetoelastic interaction energy for orthorhombic symmetry has been given in the literature.[11] Since the iron sites are crystallographically equivalent, we can write for the magnetoelastic energy density, limiting ourselves for sound propagation along the c axis,

$$\begin{aligned} E_{me} &= \epsilon_{zz}[B_{33}(\alpha_{z_1}^2 + \alpha_{z_2}^2) + B_{31}(\alpha_{x_1}^2 + \alpha_{x_2}^2) + B_{32}(\alpha_{y_1}^2 + \alpha_{y_2}^2)] \\ &\quad + \epsilon_{xz}B_{55}(\alpha_{x_1}\alpha_{z_1} + \alpha_{x_2}\alpha_{z_2}) + \epsilon_{zy}B_{44}(\alpha_{y_1}\alpha_{z_1} + \alpha_{y_2}\alpha_{z_2}) \,. \end{aligned} \tag{3}$$

Here $\alpha_{x_1}, \alpha_{x_2}, \ldots,$ are the direction cosines of the two sublattice magnetizations with respect to the orthorhombic symmetry axis, ϵ_{ij} are components of the strain tensor. Other terms involving ϵ_{xx}, ϵ_{yy}, ϵ_{xy} are omitted because we only present experimental results for c axis propagation. The B_{33}, B_{31}, and B_{32} constants are not independent of other components of the magnetoelastic tensor.[11] Since the weak ferromagnetic moment $\vec{m}$ as well as the sublattice magnetizations rotate as a function of temperature, one has to transform E_{me} to a rotated coordinate system. We choose this new coordinate system in the usual way.[8–10] Denote by T_1, S_1 and T_2, S_2 the perpendicular and parallel components of the reduced sublattice magnetization vectors in the ac plane and by Y_1, Y_2 the components in the b direction; further assume the canting angle W of the sublattice magnetizations to be small. (We shall comment on W being small below.) Then we get[8–10]

$$\begin{aligned} &\alpha_{x_1} = S_1\cos\theta - T_1\sin\theta, \quad \alpha_{x_2} = -S_2\cos\theta + T_2\sin\theta \,, \\ &\alpha_{y_1} = Y_1, \quad \alpha_{y_2} = Y_2 \,, \\ &\alpha_{z_1} = -S_1\sin\theta - T_1\cos\theta, \quad \alpha_{z_2} = S_2\sin\theta + T_2\cos\theta \,, \end{aligned} \tag{4}$$

where θ is the angle between weak ferromagnetic moment and c axis as defined in the Introduction. By considering only linear terms in T and Y we get from (3)

$$\begin{aligned} E_{me} &= \epsilon_{zz}B_{33}[(S_1^2 + S_2^2)\sin^2\theta + (S_1T_1 + S_2T_2)\sin 2\theta] \\ &\quad + \epsilon_{zz}B_{31}[(S_1^2 + S_2^2)\cos^2\theta - (S_1T_1 + S_2T_2)\sin 2\theta] \\ &\quad + \epsilon_{xz}B_{55}[-\tfrac{1}{2}(S_1^2 + S_2^2)\sin 2\theta - (S_1T_1 + S_2T_2)\cos 2\theta] \\ &\quad + \epsilon_{yz}B_{44}[-Y_1S_1\sin\theta + Y_2S_2\sin\theta] \,. \end{aligned} \tag{5}$$

B. Thermodynamic Calculation of Velocity Changes

Before we go into the rather involved equation-of-motion calculation, we present a simple calculation for the velocity change of sound waves near displacive phase transitions. Let us first consider the upper phase transition (T_u). For the equilibrium state we have $\langle S_i\rangle = 1$, $\langle T_i\rangle = \langle Y_i\rangle = 0$. We define $\tilde{E} = E(\epsilon_{ij}, \langle S\rangle, \langle Y\rangle, \langle T\rangle)$. From Eq. (5) it follows that the order-parameter–phonon coupling is quadratic in the order parameter for longitudinal waves in the vicinity of T_u; $\tilde{E}_{me} = 2\epsilon_{zz}(B_{33} - B_{31})\theta^2$. We can calculate the elastic constants by using $\tilde{E} = E_{el} + E_\theta + \tilde{E}_{me}$, Eqs. (1) and (5), and $E_{el} = \frac{1}{2}c_{33}^0\epsilon_{zz}^2$. With

$$c_{33} = \frac{\partial^2 E}{\partial\epsilon_{zz}^2}(\epsilon_{zz}, \theta(\epsilon_{zz})) \quad \text{and} \quad \frac{\partial E}{\partial\theta} = 0 \,,$$

we get for the elastic constants

$$\begin{aligned} c_{33} &= c_{33}^0 - (B_{33} - B_{31})^2/4K_b \quad \text{for } T \leq T_u \,, \\ c_{33} &= c_{33}^0 \qquad\qquad\qquad\quad \text{for } T > T_u \,, \end{aligned} \tag{6a}$$

i.e., the elastic constant c_{33} and hence the corresponding longitudinal sound velocity exhibits a steplike discontinuity at T_u. Analogously for T_l we get

$$c_{33} = c_{33}^0 - (B_{33} - B_{31})^2/4K_b \quad \text{for } T \geq T_l\,, \qquad c_{33} = c_{33}^0 \quad \text{for } T < T_l\,. \tag{6b}$$

One obtains such a result whenever the phonon–order-parameter interaction is linear in the strain, but quadratic in the order parameter. Another example of exactly such behavior are the elastic constants near the structural phase transition in $SrTiO_3$.[12–14] The equation-of-motion method presented in Sec. II C gives, for the dominant term, exactly the results of Eqs. (6). The experimental results presented below exhibit such behavior.

For the shear waves with polarization vector $\vec{R}$ along the a axis we obtain from Eq. (5) a phonon–order-parameter coupling, linear in the order parameter $\tilde{E}_{me} = -\epsilon_{xz} B_{55} 2\theta$. We therefore expect quite different behavior than in the longitudinal case. In fact, one expects that the shear-wave elastic constant becomes soft because of a frequency pulling due to this linear soft-mode–phonon interaction. An analogous calculation as in the longitudinal case gives the following:

$$c_{55} = c_{55}^0 - \frac{B_{55}^2}{(\omega_1/\gamma)^2}\,, \tag{7}$$

where ω_1 is the soft-mode frequency discussed below. The equation-of-motion method discussed below recovers essentially the same result. This is precisely what one observes experimentally for this configuration (see below).

Finally, for shear waves with polarization vector $\vec{R}$ along the b axis, we do not get any phonon–order-parameter coupling from Eq. (5). We therefore expect no drastic effects for this configuration, again borne out by the detailed calculation and by the experimental results presented below.

C. Equation-of-Motion Method

1. *Spin-Wave Spectra*

We give here the calculation of velocity and attenuation changes using the linearized coupled equations of motion for spin waves and sound waves. In this paper we treat the case of zero external field, leaving field-dependent effects to a future publication. We represent the spin system of the orthoferrite by a system of two magnetic sublattices, allowing therefore for optical spin-wave modes. In order to keep the amount of algebra to a minimum, we assume the canting angle W to be small, only considering it up to first order and we neglect the single-ion anisotropy constant A_{xz}. These simplifications do not affect our results in any significant way. In fact, the dependence of such terms on the angle θ for the soft mode is the same as one of the other anisotropy terms and therefore could be absorbed in those terms in the final result. For the optical spin-wave branch, we expect a more critical dependence on W and A_{xz}. But, since we do not use these optical modes in any crucial way, we disregard their influence. Then we get from Refs. 8–10, applying the transformation (4) for the magnetic part of the energy density,

$$\begin{aligned} E_m = {} & (S_1 S_2 + T_1 T_2)(-E - 2WD) + E Y_1 Y_2 \\ & + (2WE - D)(S_1 T_2 - S_2 T_1) \\ & - (A_{xx}\cos^2\theta + A_{zz}\sin^2\theta)(S_1^2 + S_2^2) \\ & - (T_1^2 + T_2^2)(A_{xx}\sin^2\theta + A_{zz}\cos^2\theta) \\ & + (S_1 T_1 + S_2 T_2)(A_{xx} - A_{zz})\sin 2\theta \\ & + \tfrac{1}{2}K_b[(S_1^4 - 6T_1^2 S_1^2 + S_2^4 - 6S_2^2 T_2^2)\cos 4\theta \\ & - 4S_1 T_1 (S_1^2 - T_1^2)\sin 4\theta - 4S_2 T_2 (S_2^2 - T_2^2)\sin 4\theta]\,. \end{aligned} \tag{8}$$

In this notation A_{xx} and A_{zz} are twofold anisotropy constants (related to K_u used above by $A_{xx} - A_{zz} = -\frac{1}{2}K_u$), E is the exchange constant, D is the antisymmetric exchange constant. From Eq. (8) follows the well-known fact[4] that the sublattice magnetizations and the weak ferromagnetic moment are confined to the ac plane. It is this anisotropy with respect to the b axis which makes the problem no longer axially symmetric and, therefore, the spin-wave modes soft only at temperatures T_l and T_u but not inbetween these temperatures. Apart from constant terms Eq. (8) reduces to Eq. (1) with

$$\tilde{E}_m = E_m(\langle S_i\rangle = 1,\ \langle T_i\rangle = \langle Y_i\rangle = 0)\,.$$

Applying the equation of motion to Eq. (8) and using Eq. (2) the following expressions result for the spin-wave modes (see Appendix A):

$$\begin{aligned} (\omega_1/\gamma)^2 &= (4E/M_0^2)[(A_{xx} - A_{zz})\cos 2\theta - 4K_b\cos 4\theta]\,, \\ (\omega_2/\gamma)^2 &= (4E/M_0^2)[\tfrac{1}{2}(A_{xx} + A_{zz}) + \tfrac{1}{2}(A_{xx} - A_{zz}) \\ &\quad \times \cos 2\theta - K_b\cos 4\theta]\,. \end{aligned} \tag{9}$$

Here γ is the gyromagnetic ratio. We emphasize again that taking terms in W to higher order than linear can change the expression for ω_2/γ significantly. In Fig. 1 we show the temperature dependence of ω_1/γ for typical values of the constants used. These numerical constants are listed in Table I. They represent the parameters with which we shall make quantitative numerical comparisons with our experimental results.

Although Eq. (9) gives, strictly speaking, only the $k = 0$ spin-wave modes, we can use them for

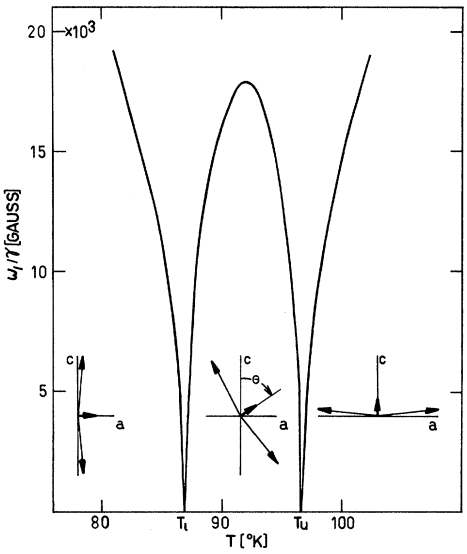

FIG. 1. Temperature dependence of soft-mode frequency ω_1/γ, calculated with the parameters from Table I [see Eq. (9)]. The spin structure for the different temperature regions is also indicated.

calculating the spin-wave–phonon interaction because typical phonon wave vectors are $k \sim 10^3$ cm^{-1}, for which the exchange terms αk^2 in the spin-wave spectrum are still negligible.

2. *Longitudinal Sound Waves Propagating in c Direction*

Next we calculate the coupled spin-wave–phonon dispersion equation for the case of longitudinal sound waves propagating along the c axis. We denote this configuration by (k_c, R_c). We use the energy expressions of Eqs. (5) and (8) plus an additional elastic energy term. Analogously to the method given in Appendix A, we can set up coupled equations of motion for the spin system. For the sound wave we also have to consider, in addition to an effective stress, $\sigma_{zz} = \partial E_{me}/\partial \epsilon_{zz}$, a volume force of the form $M_i \partial H_i^e/\partial z$. In Appendix B more details of the calculation are given. From (B2) it follows for the dominant term of the longitudinal sound velocity that

$$v = v_l - \frac{2E(B_{33}-B_{31})^2 \sin^2 2\theta}{\rho v_l M_0^2 (\omega_1/\gamma)^2} \quad . \tag{10}$$

This gives, with the aid of Eqs. (2) and (9),

$$v = v_l \quad \text{for } T < T_l \text{ and } T > T_u \, ,$$

$$v = v_l - (B_{33}-B_{31})^2/\rho v_l 8K_b \quad \text{for } T_l < T < T_u \, . \tag{11}$$

The result (11) is identical with Eq. (6) of the preceding section.

3. *Shear Waves Propagating in c Direction with Polarization Vector along a Axis*

This configuration we denote by (k_c, R_a). In analogous fashion as above, we can calculate the phonon–spin-wave dispersion spectrum for this configuration. Details of the calculation are given again in Appendix B. The result is, for small changes in the sound velocity,

$$v = v_t - B_{55}^2 \frac{E \cos^2 2\theta}{M_0^2 \rho v_t (\omega_1/\gamma)^2} \, . \tag{12}$$

Apart from modulation factors $E \cos^2 2\theta$ this result is equivalent to Eq. (7). Equation (12) has quite a different form than Eq. (11). Whereas in Eq. (10) the soft-mode parameters cancel in nominator and denominator, resulting in Eq. (11), there is only a soft-mode parameter in the denominator of Eq. (12), which makes the shear sound velocity approach zero in this particular geometry. Damping effects, among other effects discussed below, however, will only allow sharp dips in the sound velocity for this configuration. This behavior was anticipated in Sec. II B.

4. *Shear Waves Propagating in c Direction with Polarization Vector along b Axis*

This configuration we denote by (k_c, R_b). Again we defer the details of the calculation to Appendix B. For small changes in sound velocity one gets

$$v = v_s - \frac{B_{44}^2 E \sin^2 \theta}{\rho M_0^2 v_s (\omega_2/\gamma)^2} \, . \tag{13}$$

The sound velocity for this configuration is not coupled to any soft-mode parameter. The only significant temperature dependence results from $\sin^2\theta$ [Eq. (2)] and from $(\omega_2/\gamma)^2$. In principle, one can infer from (13) information regarding the optical branch of the spin-wave spectrum.

5. *Effects of Damping*

So far we have neglected any effect due to soft-mode damping. If damping is included we expect to get noticeable effects in the sound velocity and, in particular, we expect attenuation peaks to occur wherever the sound-wave and spin-wave modes get

TABLE I. Magnetic constants for $ErFeO_3$ used for the analysis (Refs. 4 and 7).

Sublattice magnetization	$M_0 = 440$ G
Exchange energy	$E = 22 \times 10^8$ erg/cm^3
Antisymmetric exchange energy	$D = 4.4 \times 10^7$ erg/cm^3
Anisotropy energy: Twofold[a]	$K_u(T) = 2.8 \times 10^5 - 3.10^3\, T$ erg/cm^3[b]
Fourfold	$K_b = 1.8 \times 10^3$ erg/cm^3
Density	$\rho = 8.07$ g/cm^3

[a] The typical values of the anisotropy constants, near the spin reorientation, were modified to fit the experimentally observed T_l and T_u [see Table II and Eq. (2)].

[b] T in °K.

close, i.e., near T_l and T_u. We introduce damping effects in a very simplified phenomenological manner, by substituting for ω_1/γ by $\omega_1/\gamma + i\Delta H$, where ΔH is a measure of the spin-wave linewidth. In this way we get at least a qualitative picture of damping effects. There are so many possible damping mechanisms present (intrinsic damping, sample inhomogeneity, phonon–spin-wave conversion losses, etc.) that a more sophisticated approach would not necessarily lead to an improvement of the description of damping.

For small damping, i.e., $\omega_1/\gamma \gg \Delta H$ and still $\omega \ll \omega_1$, we get the following expressions for the sound velocity and attenuation changes for the different sound-wave configurations after taking real and imaginary parts:

(a) longitudinal (k_c, R_c),

velocity change
$$v = v_t - \frac{2E(B_{33}-B_{31})^2 \sin^2 2\theta}{\rho M_0^2 v_t} \frac{[(\omega_1/\gamma)^2 - \Delta H^2]}{(\omega_1/\gamma)^2[(\omega_1/\gamma)^2 + 2\Delta H^2]}\ , \tag{14a}$$

attenuation
$$\alpha = \frac{2kE(B_{33}-B_{31})^2 \sin^2 2\theta\, 2\Delta H(\omega_1/\gamma)}{\rho M_0^2 v_l^2 [(\omega_1/\gamma)^4 + 2(\omega_1/\gamma)^2 \Delta H^2]}\ ; \tag{14b}$$

(b) shear wave (k_c, Ra),

velocity change
$$v = v_t - \frac{E B_{55}^2 \cos^2 2\theta}{\rho M_0^2 v_t} \frac{(\omega_1/\gamma)^2 - \Delta H^2}{(\omega_1/\gamma)^2[(\omega_1/\gamma)^2 + 2\Delta H^2]}\ , \tag{15a}$$

attenuation
$$\alpha = \frac{2kE B_{55}^2 \cos^2 2\theta}{\rho M_0^2 v_t^2} \frac{2\Delta H\, \omega_1/\gamma}{(\omega_1/\gamma)^2[(\omega_1/\gamma)^2 + \Delta H^2]}\ . \tag{15b}$$

For shear-wave propagation with polarization vector in the b direction we do not expect any damping effects, since ω_1 does not enter Eq. (13).

III. EXPERIMENT

We shall give experimental results for $ErFeO_3$ which exhibits the spin reorientation phenomenon in the temperature region from 86 to 97 °K approximately. The single crystals were grown by a flux method[15] at the Weizmann Institute. The crystal used in this research has dimensions of 8.9×3×3 mm with its longest axis coinciding with the crystallographic c axis. Magnetization data on crystals of the same batch gave magnetic constants in accordance with previous data.[16] Relevant data on these crystals are gathered in Table I.

The two end faces of the crystal used were polished plane parallel to within optical accuracy. Sound-wave propagation was studied in the frequency range 30–170 MHz. Except for the vicinity of the transition temperatures, the echo pattern was perfect, exhibiting more than 20 echos. The velocity was measured using a phase comparison method described previously.[17] Its resolution in the present case was 1 ppm. A modulated echo pattern, as is present in the vicinity of the transition temperatures, does not affect the accuracy of these velocity measurements, since our method employs a single echo at constant amplitude. The sound-wave attenuation was measured using a calibrated attenuator. In this case the echo pattern modulation affects the accuracy of the attenuation measurements. Therefore, we took averages over different echo amplitude differences, indicating in the figures the spread of possible values by error bars.

The temperature was monitored using a heater arrangement with feedback provisions.[18] We could read the temperature and keep it constant to 10 mdeg.

In Table I we list all pertinent physical constants of the $ErFeO_3$ crystal. It should be noted that the quoted values vary in their reliability, especially K_u and K_b are representative values only, since these constants for $ErFeO_3$ are not known. However, they were adjusted [Eq. (2)] as to give phase-transition temperatures at $T_l = 87$ °K and $T_u = 96.6$ °K, respectively.

We investigated three different sound-wave propagation configurations as mentioned above: (a) longitudinal (k_c, R_c), (b) shear wave with polarization vector along the a axis (k_c, R_a), and (c) shear wave with polarization vector along the b axis (k_c, R_b).

IV. RESULTS AND DISCUSSION

An over-all temperature dependence of the three sound velocities for the temperature region 77–300 °K is shown in Fig. 2. The absolute values of the sound velocities at 300 °K are given in Table II. The shear-wave velocity for the (k_c, R_a) configuration shows even outside the spin reorientation region a rather unexpected temperature dependence. This might be connected with the anomalous tem-

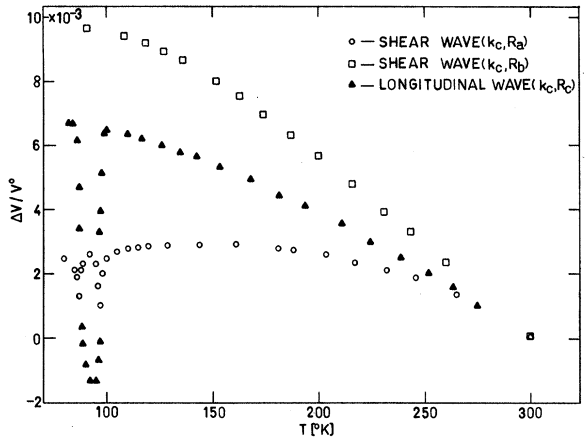

FIG. 2. Temperature dependence of the sound velocity changes $\Delta v/v^0$ for the three configurations between 80 and 300 °K, normalized at $T = 300$ °K. The absolute values of v^0 (300 °K) are listed in Table II.

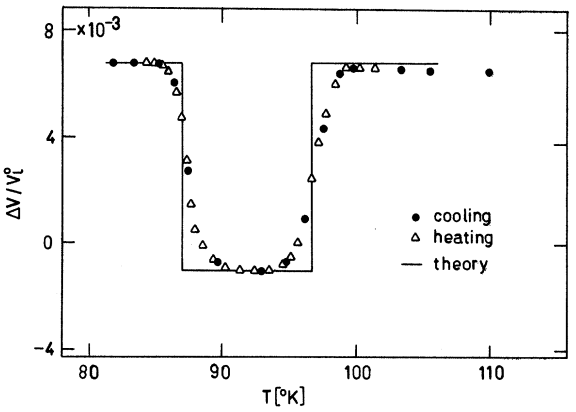

FIG. 3. Longitudinal velocity changes for the configuration (k_c, R_c) in the phase-transition region for 30-MHz sound waves. Solid line denotes theoretical result. v_t^0 is the sound velocity at room temperature (Table II).

perature dependence of the weak ferromagnetic moment in this region.[4] In the following we shall present and discuss the data in the phase-transition region.

A. Longitudinal Sound Velocity

In Fig. 3 we show more detailed data for the sound velocity in the phase-transition region. The data was taken both by lowering and by raising the temperature, thus ensuring that true second-order transition behavior with no hysteresis effects was present. The data shown in Fig. 3 clearly display the features anticipated in Sec. II, namely, a step-like discontinuity at the upper and lower phase-transition temperatures. In fact, the transition is somewhat broadened over ~ 2 °K. This can be due to a number of reasons, the main one being sample inhomogeneities. Although soft-mode damping could also give rise to such a broadening [Eq. (14b)], the value for the spin-wave linewidth, $\Delta H \sim 100$ Oe, fitted to the attenuation data, is much too small to account for this effect. From Fig. 3 one infers transition temperatures of $T_u \sim (98 \pm 1)$°K and $T_l \sim (86 \pm 1)$°K. In fact, the shear-wave data presented in Fig. 4 give, with a better accuracy, $T_u = 96.6$ °K and $T_l = 87$ °K. At these temperatures one can actually see a kink in the slope of the velocity curves of Fig. 3. Depending on which choice of transition temperatures one takes, the total velocity change at the two transition temperatures is 0.6–0.8%. We use the bigger value of 0.8% for the evaluation, ascribing this small ambiguity again to the broadening of the transition. With Eqs. (6) or (11) and the parameters listed in Tables I and II we obtain for the effective magnetoelastic coupling constant $|B_{33} - B_{31}| \sim 18 \times 10^6$ erg/cm^3. There are no magnetoelastic coupling constants or magnetostriction constants available from other measurements for this substance. In all the experiments an applied field of ~ 50 Oe, applied in the *ac* plane while creating a nearly single domain state, did not change this zero-field result shown in Fig. 3, excluding any possible domain effects.

TABLE II. Constants, deduced from this experiment.

Transition temperatures[a]	$T_l = 87$ °K, $T_u = 96.6$ °K
Longitudinal sound velocity associated with	c_{33} ($T = 300$ °K), $v_l = 5.85 \times 10^5$ cm/sec
Shear sound velocity associated with	c_{55} ($T = 300$ °K), $v_t = 3.33 \times 10^5$ cm/sec
Shear sound velocity associated with	c_{44} ($T = 300$ °K), $v_s = 3.83 \times 10^5$ cm/sec
Magnetoelastic coupling constants	$\lvert B_{33} - B_{31} \rvert = 18 \times 10^6$ erg/cm^3
	$\lvert B_{55} \rvert = 2.2 \times 10^6$ erg/cm^3

[a]The values for T_l and T_u were determined from Fig. 4.

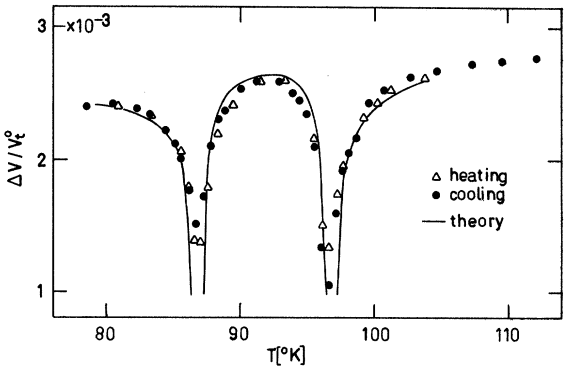

FIG. 4. Shear-wave velocity change for the configuration (k_c, R_a) in the phase-transition region for 50-MHz sound waves. Solid line denotes theoretical result. v_t^0 is the sound velocity at room temperature (Table II).

B. Shear Waves with Polarization Vector in *a* Direction

Figure 4 shows velocity changes occurring for shear waves in the configuration (k_c, R_a). In contrast to the longitudinal sound-wave result, we observe pronounced dips in the sound velocity at the transition temperatures T_l and T_u. As in the longitudinal case it is a beautiful manifestation of the particular phonon–soft-mode coupling as discussed in Sec. II. We can again take the representative material constants from Table I and fit the experimental curve by taking $|B_{55}| \sim 2.2\times10^6$ erg/cm^3 using Eq. (12). This gives a fit in reasonable agreement with experiment. Use of the alternative equation (15a), with damping included, again gives a fit indistinguishable from the one just discussed except very close to T_l and T_u. Again we can conclude that it is not a reasonable soft-mode linewidth of $\Delta H \sim 100$ Oe but rather again sample inhomogeneities which probably account for the partial smearing out of the dips in the vicinity of T_l and T_u. Temperature cycling for this case also did not reveal any hysteresis effects, thereby excluding again observable first-order phase-transition effects. In addition, an applied field of 50 Oe again did not give any change of the zero-field data, eliminating possible domain effects. It should be noted that the velocity dip at T_l is noticeably smaller than the one at T_u. This experiment is by far the most accurate one to determine T_l and T_u.

C. Shear Waves with Polarization Vector in *b* Direction

Finally, in Fig. 5 we show velocity data for shear waves in configuration (k_c, R_b). For this geometry we predicted no spectacular effects, only a coupling of the sound wave to the optical spin-wave mode, which does not become soft. A rather smooth temperature dependence of the velocity

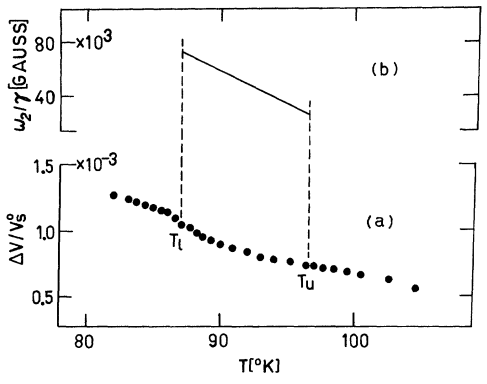

FIG. 5. (a) Shear-wave velocity change for the configuration (k_c, R_b) in the phase-transition region for 50-MHz sound wave. v_s^0 is the sound velocity at room temperature (Table II). (b) Temperature dependence of the optical spin-wave mode using results of (a) and Eq. (13).

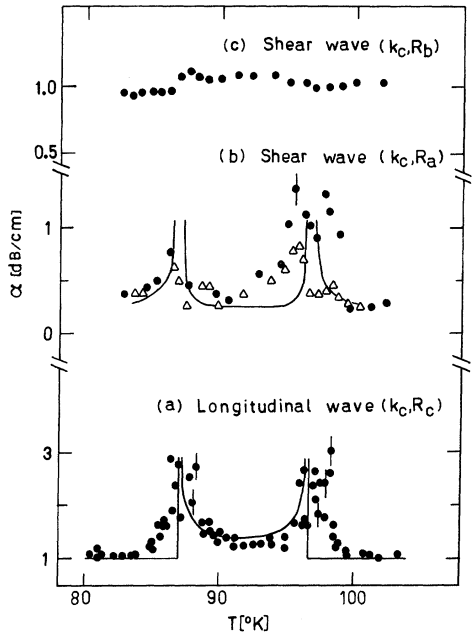

FIG. 6. Sound-wave attenuation changes in the spin reorientation region for the three different configurations. ●: 50 MHz, Δ: 30 MHz. Solid lines denote theoretical result using Eqs. (14b) and (15b).

change is indeed observable from the data in Fig. 5. Equation (13) predicts a change in the sound velocity at T_l because of the modulation factor $\sin^2\theta$ which is 1 for $T < T_l$ but decreases continuously for $T > T_l$ till it reaches 0 for $T = T_u$. With a reasonable value of $B_{44} \sim 4\times10^6$ erg/cm^3 we have determined the temperature dependence of ω_2 using Eq. (13). As already pointed out in Appendix A, this provides one experiment to determine ω_2, for cases where other methods fail. However, as stressed before, our various approximations, discussed in Sec. II, make the predicted optical spin-wave frequency result only a qualitative one.

D. Attenuation Experiments

Figure 6 shows ultrasonic attenuation data for the three sound-wave propagation configurations. It can be seen that for the configurations (k_c, R_c) and (k_c, R_a) attenuation peaks in the vicinity of the transition temperatures T_l and T_u show up. For the (k_c, R_b) configuration only a small step near T_l, probably arising from a misalignment of our transducer and again from the modulation factor $\sin^2\theta$, appears. From Fig. 6 one can see that the attenuation peak at T_l is noticeably smaller than the one at T_u for the shear-wave case. A corresponding asymmetry was also found in the velocity dips for this configuration (see Fig. 4). Actually, the attenuation peaks seem to display some structure

as seen in Fig. 6. We have no satisfactory explanation for this asymmetry and structure. Error bars for the results close to T_l and T_u indicate the relative inaccuracy due to echo pattern modulation, as explained before. These observations are in qualitative agreement with our predictions (14b) and (15b). For the configuration where there is an attenuation peak, we attempted to fit Eqs. (14b) and (15b) to the experimental results, using the same constants from Tables I and II used in the fits for the velocity curves with a damping linewidth of $H \sim 100$ Oe. For the shear-wave configuration (k_c, R_a) we get a fit shown in Fig. 6 which is in rough qualitative agreement with the experiment. For the longitudinal configuration, however, theory predicts no attenuation for $T < T_l$ and $T > T_u$, the higher symmetry phases. This is the same situation as in the longitudinal velocity case. This discrepancy can probably again be explained by sample inhomogeneities. Again domain effects can be ruled out, because a small magnetic field of 50 Oe did not change any of the attenuation curves.

Equations (14b) and (15b) predict a frequency dependence which is approximately obeyed by our experiments, as shown in Fig. 6 for the shear-wave configuration (k_c, R_a) and other results up to 170 MHz not shown in the graph. No attempt is made, however, to check this frequency dependence in great detail, since our data are not good enough to warrent such an effort, as was usually done in the case of order-disorder phase transitions.[2]

On the whole, it is encouraging that our attenuation experiments can be explained at least qualitatively by taking the same constants used for the velocity effects.

V. CONCLUSION

We have shown in this paper, both experimentally and theoretically, how a sound wave interacts with a soft mode near a displacive phase transition. A resonant interaction between the sound wave and the soft spin-wave mode exhibits a variety of effects for different sound-wave configurations which have been observed and shown in this paper for the spin reorientation phase transition. (a) A longitudinal sound wave, having a magnetoelastic coupling linear in the strain and quadratic in the order parameter, exhibits steplike discontinuities in the sound velocity near the phase transition. This has been experimentally observed in the case of the spin reorientation phase transition, as discussed in this paper, as well as in the case of a structural phase transition such as the one occurring[14] in $SrTiO_3$ near $T_a \sim 106\,^{\circ}K$. This velocity effect is accomplished by an attenuation peak. (b) A shear wave having a linear phonon–order-parameter coupling becomes soft at a displacive phase transition. The reason for it is the magnetoelastic coupling which pulls the phononlike branch of the coupled magnetoelastic wave down as the soft mode approaches zero frequency. Damping effects and sample inhomogeneities make the sound-wave velocity changes finite. These velocity dips are accompanied by attenuation peaks, both of which were observed in good agreement with theoretical prediction. This effect has no counterpart in structural phase transitions. (c) Shear waves in the configuration (k_c, R_b) have no coupling to the soft mode. In this case a coupling to the optical branch of the spin-wave spectrum is predicted and also borne out by our experimental results.

It seems that our description of a resonant phonon–soft-mode interaction can explain all of our experimental results very well. The good agreement between theory and experiment implies that this resonant interaction is the dominant mechanism for all these effects. One could think of other coupling mechanisms applicable to these effects. One of these would be a higher-order coupling in the spin-wave variables, i.e., spin-wave scattering via phonon creation and absorption. Since the spin-wave mode becomes soft this effect could lead even to singularities in the attenuation and velocity changes. However, since this spin reorientation phase transition is a true Landau-type phase transition with a critical region only very near to the transition temperature[5] T_a $[(T - T_a)/T_a \sim 10^{-8}]$, this effect would become apparent only in the close vicinity of T_a. However, sample inhomogeneities, among other effects, make it impossible to observe such effects. Similar considerations hold for the structural phase transition in $SrTiO_3$ although there the critical region can occur for larger values of $(T - T_a)/T_a$.

Externally applied magnetic fields, larger than the ones described in this paper, introduce an energy gap in the soft spin-wave mode. Depending on the direction of the field the energy gap is larger at one of the two transition temperatures. This effect can easily be observed both for attenuation and velocity changes. One observes a decrease in the elastic effect (velocity or attenuation anomaly) due to an increase in the corresponding energy gap of the soft mode. These effects will be discussed in detail elsewhere.[22]

Finally, it should be mentioned that the spin reorientation phenomena are rather general phenomena in magnetic solids. Although the elastic effects in the orthoferrites are particularly striking, as shown in this paper, because of the existence of two transition temperatures, weak ferromagnetic moment and spin rotation in a plane, similar effects have or can be observed in other materials such as, e.g., Gd,[19] $NdCo_5$,[20] and Mn_2Sb.[21] A similar analysis of the results in these substances will be given elsewhere.[22]

ACKNOWLEDGEMENT

The authors would like to thank T. J. Moran for technical assistance.

APPENDIX A

The equation of motion for the spin system is given by

$$\frac{dM_i}{dt}=(\gamma\vec{M}\times\vec{H}^e)_i \ , \tag{A1}$$

where

$$\frac{M_i}{M_0}=(T_i, Y_i, S_i), \quad H_i^e=-\frac{\partial E_m}{\partial M_i} \ ,$$

and M_0 is the magnitude of the sublattice magnetization. This leads to the following determinant for the variables (T_1, T_2, Y_1, Y_2) from the linearized equations of motion:

$$\begin{vmatrix} \frac{i\omega}{\gamma}M_0 & 0 & -a & E \\ 0 & \frac{i\omega}{\gamma}M_0 & E & -a \\ -c & E & \frac{i\omega}{\gamma}M_0 & 0 \\ E & -c & 0 & \frac{i\omega}{\gamma}M_0 \end{vmatrix} = 0 \ , \tag{A2}$$

where

$$a=-E-2A_{xx}\cos^2\theta-2A_{zz}\sin^2\theta+2K_b\cos4\theta \ ,$$

$$c=E+2(A_{xx}-A_{zz})\cos2\theta-8K_b\cos4\theta \ .$$

With $E \gg A_{xx}, A_{zz}, K_b$ we obtain Eq. (9) of the main text. It should be noted that only $A_{xx}-A_{zz}=-\frac{1}{2}K_u$ can be obtained from static or resonance experiments, but not the individual A_{xx} and A_{zz}. In Appendix B we will show that certain sound-wave modes can couple to the optical spin-wave mode, providing us, at least, in principle, with a method to determine the individual A_{xx}, A_{zz}. Note that an electromagnetic field couples only weakly to the optical mode because $\gamma_1 \sim \gamma_2$ for the iron sites in the two sublattices.

APPENDIX B

1. Longitudinal Wave

The contribution to the volume force is

$$\frac{M_i}{M_0}\frac{\partial H_i^e}{\partial z}=-ik\,T_i\left[(A_{xx}-A_{zz})\sin2\theta-6K_b\sin4\theta\right] - ik\,T_{j\neq i}(2WE-D) + 2k\,R_z(B_{33}\sin^2\theta+B_{31}\cos^2\theta) \ ,$$

with R_z the sound-wave displacement component and assuming R_z, T_i, Y_i proportional to $e^{-i(\omega t-kz)}$. The determinant for the variables $(T_1, T_2, Y_1, Y_2, R_z)$ reads

$$\begin{vmatrix} \frac{i\omega}{\gamma}M_0 & 0 & -a & E & 0 \\ 0 & \frac{i\omega}{\gamma}M_0 & E & -a & 0 \\ -c & E & \frac{i\omega}{\gamma}M_0 & 0 & -l \\ E & -c & 0 & \frac{i\omega}{\gamma}M_0 & -l \\ g+h+l & g+h+l & 0 & 0 & \omega^2-v_l^2k^2+f \end{vmatrix} = 0 \ , \tag{B1}$$

with a and c defined in Appendix A, v_l is the longitudinal sound velocity

$$f=(4k^2/\rho)(B_{33}\sin^2\theta+B_{31}\cos^2\theta) \ ,$$

$$g=-ik\left[(A_{xx}-A_{zz})\sin2\theta-6K_b\sin4\theta\right] + ik\,(B_{33}-B_{31})\sin2\theta \ ,$$

$$h=ik\,(2WE-D) \ , \quad l=ik\,(B_{33}-B_{31})\sin2\theta \ .$$

Solving (B1) gives

$$(\omega^2-v_l^2k^2+f)(\omega^2-\omega_1^2)(\omega^2-\omega_2^2)+2\gamma^4 l\,(l+g)(E-a)\left[(\omega/\gamma)^2+(E+a)(E+c)\right]=0 \ ,$$

and from this we get for the longitudinal phase velocity in the limit $\omega \ll \omega_1, \omega_2$,

$$v^2=v_l^2-\frac{4}{\rho}(B_{33}\sin^2\theta+B_{31}\cos^2\theta)-\frac{4E}{\rho M_0^2}\frac{(B_{33}-B_{31})^2\sin^2\theta}{(\omega_1/\gamma)^2}+\frac{4E\,(B_{33}-B_{31})}{\rho M_0^2(\omega_1/\gamma)^2}\left[(A_{xx}-A_{zz})\sin2\theta-6K_b\sin4\theta\right]. \tag{B2}$$

In this expression the third term on the right-hand side is the dominant term. For our frequency range $\omega/\gamma < 30$ G. Using $B \simeq 10^7$ erg/cm^3 and the values listed in Tables I and II (in cm^2/sec^2) we get

$$v_l^2=35\times10^{10} \ , \quad 4B/\rho<10^7 \ , \quad \frac{4EB^2}{\rho M_0(\omega_1/\gamma)^2}\sim10^{10}$$

and the last term $\sim 10^7$, so only the third term gives a noticeable contribution.

2. Shear Waves in (k_c, R_a) Configuration

In this case there is no volume force acting on the sound wave. From Eqs. (5) and (8) we again get the determinant for the linearized equations of motion in the variables T_1, T_2, Y_1, Y_2, R_a,

$$\begin{vmatrix} \frac{i\omega}{\gamma}M_0 & 0 & -a & E & 0 \\ 0 & \frac{i\omega}{\gamma}M_0 & E & -a & 0 \\ -c & E & \frac{i\omega}{\gamma}M_0 & 0 & \frac{1}{2}(ik)B_{55}\cos2\theta \\ E & -c & 0 & \frac{i\omega}{\gamma}M_0 & \frac{1}{2}(ik)B_{55}\cos2\theta \\ -\frac{ik}{\rho M_0}B_{55}\cos2\theta & -\frac{ik}{\rho M_0}B_{55}\cos2\theta & 0 & 0 & \omega^2 - v_t^2k^2 \end{vmatrix} = 0 , \tag{B3}$$

which upon evaluation gives

$$(\omega^2 - v_t^2k^2)(\omega^2 - \omega_1^2)(\omega^2 - \omega_2^2) - \frac{B_{55}^2\cos^2 2\theta\, k^2\gamma^4}{\rho}\left[2E\left(\frac{\omega}{\gamma}\right)^2 + (E+c)(E^2 - a^2)\right] = 0 .$$

Here v_t is the shear-wave velocity for this configuration. In the limit $\omega \ll \omega_1, \omega_2$ Eq. (12) of the main text results.

3. Shear Waves in (k_c, R_a) Configuration

From the energy expressions (5) and (8) we get the determinant for the linearized equations in the variables T_1, T_2, Y_1, Y_2, R_b,

$$\begin{vmatrix} \frac{i\omega}{\gamma}M_0 & 0 & -a & E & \frac{1}{2}(ik)B_{44}\sin\theta \\ 0 & \frac{i\omega}{\gamma}M_0 & E & -a & \frac{1}{2}(ik)B_{44}\sin\theta \\ -c & E & \frac{i\omega}{\gamma}M_0 & 0 & 0 \\ E & -c & 0 & \frac{i\omega}{\gamma}M_0 & 0 \\ 0 & 0 & -\frac{ik}{\rho M_0}B_{44}\sin\theta & \frac{ik}{\rho M_0}B_{44}\sin\theta & \omega^2 - v_s^2k^2 \end{vmatrix} = 0 , \tag{B4}$$

which upon evaluation gives

$$(\omega^2 - v_s^2k^2)(\omega^2 - \omega_1^2)(\omega^2 - \omega_2^2) - \frac{B_{44}^2\sin^2\theta\, k^2\gamma^4}{\rho}\left[\left(\frac{\omega}{\gamma}\right)^2(E+c) + (a-E)(E^2 - c^2)\right] = 0 .$$

Here, v_s is the shear-wave velocity for this configuration. In the limit $\omega \ll \omega_1, \omega_2$ Eq. (13) of the main text results.

---

†Work supported by the National Science Foundation.

*On leave from Weizmann Institute of Science, Rehovoth, Israel.

[1]For a review of different phase transitions see, for example, C. W. Garland, in *Physical Acoustics*, (Academic, New York, 1970), Vol. VII.

[2]B. Lüthi, T. J. Moran, and R. J. Pollina, J. Phys. Chem. Solids 31, 1741 (1970).

[3]For a discussion of displacive Landau transitions and order-disorder transitions see L. P. Kadanoff, W. Götze, D. Hamblen, R. Hecht, E.A.S. Lewis, V. V. Palciauskas, M. Rayl, J. Swift, D. Asphres, and J. Kane, Rev. Mod. Phys. 39, 395 (1967); L. Tisza, *Phase Transformations in Solids* (Wiley, New York, 1951), p. 18; A. Zussmann and S. Alexander, J. Chem. Phys. 49, 3792 (1968).

[4]For a review of the magnetic properties of orthoferrites see D. Treves, J. Appl. Phys. 36, 1033 (1965); R. L. White, *ibid.* 40, 1061 (1969); G. Gorodetsky, *Proceedings of the Chania Conference*, 1969 (Gordon and Breach, New York, to be published), Vol. 8.

[5]L. M. Levinson, M. Luban, and S. Shtrikman, Phys. Rev. 187, 715 (1969).

[6]G. Gorodetsky, L. M. Levinson, S. Shtrikman, D. Treves, and B. M. Wanklyn, Phys. Rev. 187, 637 (1969).

[7]K. P. Belov, R. A. Volkov, B. P. Goranskii, A. M. Kadomtseva, and V. V. Uskov, Soviet Phys. Solid State 11, 935 (1969); E. M. Gyorgy, J. P. Remeika, and F. B. Hagedorn, J. Appl. Phys. 39, 1369 (1968).

[8]G. Cinader, Phys. Rev. 155, 453 (1967).

[9]J. R. Shane, Phys. Rev. Letters 20, 728 (1968).

[10]F. B. Hagedown and E. M. Gyorgy, Phys. Rev. 174,

540 (1968).
[11]W. I. Dobrov, Phys. Rev. 134, A734 (1964).
[12]E. Pytte, Phys. Rev. B 1, 924 (1970).
[13]J. C. Slonczewski and H. Thomas, Phys. Rev. B 1, 3599 (1970).
[14]B. Lüthi and T. J. Moran, Phys. Rev. B 2, 1211 (1970).
[15]B. M. Wanklyn (private communication).
[16]Z. Friedman, G. Gorodetsky, H. Shaked, and S. Shtrikman (unpublished).
[17]T. J. Moran and B. Lüthi, Phys. Rev. 187, 710 (1969).
[18]R. J. Pollina, thesis, Rutgers University, 1970 (unpublished).
[19]M. Long, A. R. Wazzan, and R. Stern, Phys. Rev. 178, 775 (1969); T. J. Moran and B. Lüthi, J. Phys. Chem. Solids 31, 1735 (1970).
[20]H. Bartholin, B. van Laar, R. Lemaire, and J. Schweizer, J. Phys. Chem. Solids 27, 1287 (1966).
[21]F. J. Darnell, W. H. Cloud, and H. S. Jarrett, Phys. Rev. 130, 647 (1963).
[22]G. Gorodetsky, B. Lüthi, and T. J. Moran, in Proceedings of Soridan Conference on Dynamical Aspects of Critical Phenomena, 1970 (unpublished), p. 293.

PHYSICAL REVIEW B VOLUME 2, NUMBER 9 1 NOVEMBER 1970

Transient Fields in Ferromagnetic Iron and Gadolinium

G. M. Heestand* and P. Hvelplund
Institute of Physics, University of Aarhus, Denmark

and

B. Skaali† and B. Herskind
The Niels Bohr Institute, University of Copenhagen, Denmark

(Received 16 June 1970)

Experiments studying the velocity dependence of the transient field for ^{196}Pt in Fe and the transient field for ^{194,196,198}Pt in Gd have been carried out in order to make comparisons with the recent Lindhard-Winther theory. Agreement between theory and experiment is good concerning the shape of the velocity dependence, but the experimental value is a factor of 2 larger than theoretically predicted. A large precession due to the transient field ($\phi = -51 \pm 7$ mrad) has been found for Pt in Gd. A transient field precession for Pd and Cd in Gd has been computed on the basis of recent radioactivity results. The internal field for Pt in Gd has been measured to be -780 ± 120 kG, while former internal field values for Mo, Ru, and Hf in Gd have been corrected for transient field effects.

I. INTRODUCTION

Recent angular precession measurements[1,2] of nuclei implanted into polarized ferromagnetic backings using the ion-implantation perturbed-angular-correlation technique (IMPAC) have shown the existence of a large positive magnetic field. This field is several megagauss in magnitude, parallel to the external field, and acts for a time shorter than 1 psec. The origin of this so-called transient field is now believed to be due to the scattering of polarized electrons by the recoiling ion.

Lindhard and Winther,[3] using the idea of electron scattering, have formulated a transient field theory in which they predict the magnitude and velocity dependence of the transient field acting on different nuclei recoiling through different ferromagnetic backings. The basic parameters of the Lindhard-Winther theory which can be tested experimentally are the transient field's dependence upon the recoiling ion's velocity and the dependence upon polarized electron density in the ferromagnetic backing. The former was tested by measuring the angular precession of ^{196}Pt implanted into Fe at different velocities, while the latter was tested by measuring the angular precession of ^{194,196,198}Pt implanted into Gd.

II. EXPERIMENTAL TECHNIQUE AND RESULTS

IMPAC has been described in detail in previous publications.[1,4] In the present experiment, heavy-ion beams of oxygen and sulfur ions are used to Coulomb excite and concurrently implant platinum nuclei into a ferromagnetic backing.

Upon entering the ferromagnetic backing, the recoiling nuclei experience a large aligned time-dependent magnetic field $H(t)$. The excited nuclei then precess with the Larmor frequency $\omega(t) = -g\mu_N H(t)/\hbar$, where g is the nuclear g factor and μ_N is the nuclear magneton. After the nuclei become stationary in the lattice, $H(t)$ becomes constant in time. The only time dependence comes from the transient field which is assumed to be zero after the ion stops. Integrating $\omega(t)$ over the lifetime τ of the excited state and assuming that no excited nuclei decay in flight, one obtains the integral precession